

See discussions, stats, and author profiles for this publication at: <https://www.researchgate.net/publication/42107977>

Long-Range Energy Propagation in Nanometer Arrays of Light Harvesting Antenna Complexes

ARTICLE *in* NANO LETTERS · MARCH 2010

Impact Factor: 13.59 · DOI: 10.1021/nl1003569 · Source: PubMed

CITATIONS

36

READS

45

8 AUTHORS, INCLUDING:



Yiping Zhao

Materiomics bv, Enschede, Netherlands

13 PUBLICATIONS 197 CITATIONS

[SEE PROFILE](#)



Jurriaan Huskens

University of Twente

365 PUBLICATIONS 8,282 CITATIONS

[SEE PROFILE](#)



Vinod Subramaniam

VU University Amsterdam

270 PUBLICATIONS 5,950 CITATIONS

[SEE PROFILE](#)



Cees Otto

University of Twente

231 PUBLICATIONS 5,241 CITATIONS

[SEE PROFILE](#)

Long-Range Energy Propagation in Nanometer Arrays of Light Harvesting Antenna Complexes

Maryana Escalante,[†] Aufried Lenferink,[‡] Yiping Zhao,^{§,||} Niels Tas,^{||} Jurriaan Huskens,[§] C. Neil Hunter,[‡] Vinod Subramaniam,^{*,†} and Cees Otto^{*,†}

[†]Nanobiophysics, [‡]Medical Cell Biophysics, [§]Molecular Nanofabrication, and ^{||}Transducers Science and Technology, MESA+ Institute for Nanotechnology, University of Twente, P.O. Box 217, 7500 AE Enschede, The Netherlands and

[‡]Department of Molecular Biology and Biotechnology, University of Sheffield, Sheffield S10 2TN, U.K.

ABSTRACT Here we report the first observation of long-range transport of excitation energy within a biomimetic molecular nanoarray constructed from LH2 antenna complexes from *Rhodobacter sphaeroides*. Fluorescence microscopy of the emission of light after local excitation with a diffraction-limited light beam reveals long-range transport of excitation energy over micrometer distances, which is much larger than required in the parent bacterial system. The transport was established from the influence of active energy-guiding layers on the observed fluorescence emission. We speculate that such an extent of energy migration occurs as a result of efficient coupling between many hundreds of LH2 molecules. These results demonstrate the potential for long-range energy propagation in hybrid systems composed of natural light harvesting antenna molecules from photosynthetic organisms.

KEYWORDS Energy propagation, excitonic transport, light harvesting complexes, nanoimprint lithography, host–guest interactions

The capability to manipulate biomolecules with nanometer precision on surfaces in a massively parallel fashion is an important strategy to create complex novel hybrid structures with physical and chemical¹ properties and performance beyond those currently envisioned in, for example, energy storage and optical applications. In this context, purified components of photosynthetic organisms have been proposed as molecules for integration in solid-state electronic devices,² for the creation of patterned fluorescent nanoarrays,^{3,4} and for application in sensing devices.^{2,5,6} The nanomachinery of the photosynthetic bacterium *Rhodobacter* (*Rb.*) *sphaeroides* has been a valuable model and object of many studies for diverse aspects of biophysics, biochemistry and molecular biology. Such studies span a wide range of topics, including bacteriochlorophyll (BChl) biosynthesis, membrane assembly, secondary electron transfer, molecular genetics, reaction center structure and photochemistry, and light harvesting structure, mutagenesis, and spectroscopy.⁷ Although a large variety of photosynthetic organisms exist, which can be distinguished by their typical light harvesting antennas and electron transport system, they have in common basic principles of energy transport. The photosynthetic antenna–protein complexes collect solar energy and transfer electronic excitation energy to the photosynthetic reaction center, where charge separation occurs.⁸ In *Rb. sphaeroides* the antenna LH2

complex is built of nine identical subunits each consisting of an α and a β polypeptide. The LH2 α polypeptides form an inner ring surrounded by the β ring. In total 27 BChl molecules are bound to this structure of which 18 BChl make up the B850 system and 9 BChl interact to form the B800 system.⁹ The LH2 complex has dimensions of ~6.8 nm in height and ~7 nm in diameter.¹⁰ In *Rb. sphaeroides* LH2 transfers energy to the RC via the LH1 complex, which surrounds the RC. The (RC-LH1-PufX)₂ dimer complex consists of 28 $\alpha\beta$ protomers and 56 B875 BChls, the dimensions of which are ~11.5 \times 23 nm and ~9.4 nm in height.^{11,12} The purified components of the photosynthetic unit are interesting candidates for the fabrication of photonic structures in nanotechnology, which might find applications in synthetic light converting constructs, because of their well-defined optical properties, such as a broad spectral range, high absorption cross section, efficient energy transfer, and high photostability.^{13,14}

The unique capability of light harvesting molecules to efficiently guide energy to the reaction center has been extensively investigated.^{14–16} In particular the very early events in energy transfer from carotenoids to the B800 and B850 ring systems have been well established.¹⁷ It has been proposed that typically within ~100 ps^{18,19} an excitation arrives at the reaction center.

The actual organization of bacterial photosynthetic membranes has been revealed by atomic force microscopy (AFM).^{20–22} Although significant variation in organization occurs, it was observed that close connections between LH2 and LH1 occur most frequently.²⁰ It can therefore be con-

* To whom correspondence should be addressed. c.otto@utwente.nl and v.subramaniam@utwente.nl.

Received for review: 01/31/2010

Published on Web: 03/16/2010

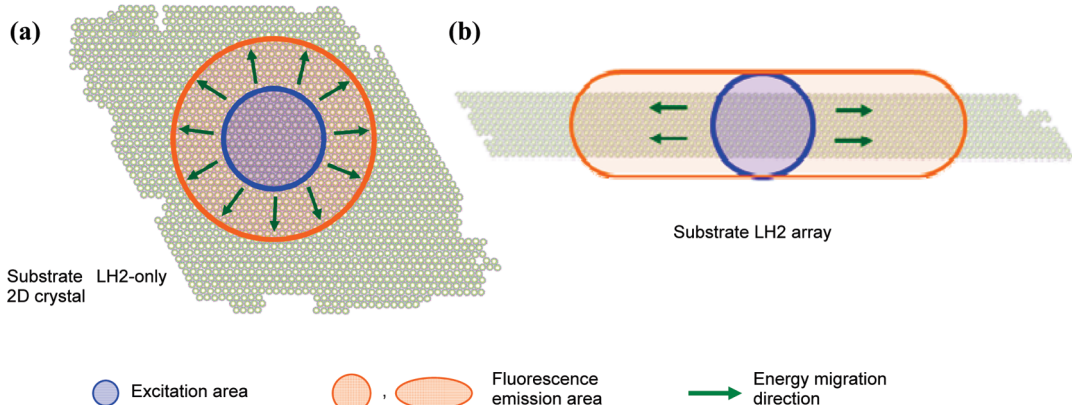


FIGURE 1. A schematic representation of different LH2 substrates used for energy migration experiments: (a) lipid reconstituted LH2 2D crystal; (b) nanometer array of LH2 complexes. The figure depicts how, upon local excitation (blue area, not to scale with respect to the LH2 molecules), the fluorescent emission (orange area) varies depending on the geometry of an active guiding layer. For crystals the fluorescent emission spreads isotropically along the surface; however on the nanometer line arrays the propagation follows the structure of the molecular organization.

cluded from the high-resolution AFM data that the distances for excitons to travel are generally small and of the order of 4 nm for nearest neighbor complexes and up to 50 nm for extended systems, such as bacterial photosynthetic vesicles.¹⁹ So, although LH2 and LH1 have exquisite properties for light transport, it is by no means obvious that these systems are suitable for long-range energy transport.

In this work, we report for the first time the direct observation of long-range transport in synthetic nanometer arrays of natural light harvesting antenna LH2 from *Rb. sphaeroides*. The arrays are ~80 nm wide and several micrometers in length. We emphasize in particular the extremely long-range energy transport that we observe in a significant fraction of events. We used two different LH2 assemblies for energy propagation experiments: LH2-only 2D crystals and engineered quasi-1D nanometer arrays of LH2 fabricated on chemically functionalized substrates. Our experimental far-field optical results, acquired with an excitation wavelength of 800 nm, show that energy is transported away from the excitation point by the ordered natural antennas. The analysis examines the influence of active energy-transporting layers on the observed fluorescence emission area (Figure 1). In the absence of light transport, a narrow diffraction limited fluorescence emission area results, while in the presence of transport the fluorescence emission area is broadened by molecular transport of excitons, which causes the emission of light at a distance away from the excitation point. We selected lipid reconstituted LH2 crystals of sufficient size ($>4\ \mu\text{m}$ in x and y directions), much larger than the size of the area excited by the focused laser beam, which is $0.45\ \mu\text{m}$ in diameter. Such crystals can be considered as two-dimensional light harvesting arrays. The fluorescence emission appears as a circular profile due to this 2D arrangement. In engineered 80 nm wide line arrays, the fluorescence emission area follows the geometry of the lines. For measurements under ambient oxygen concentration, a decrease was observed in the extent of

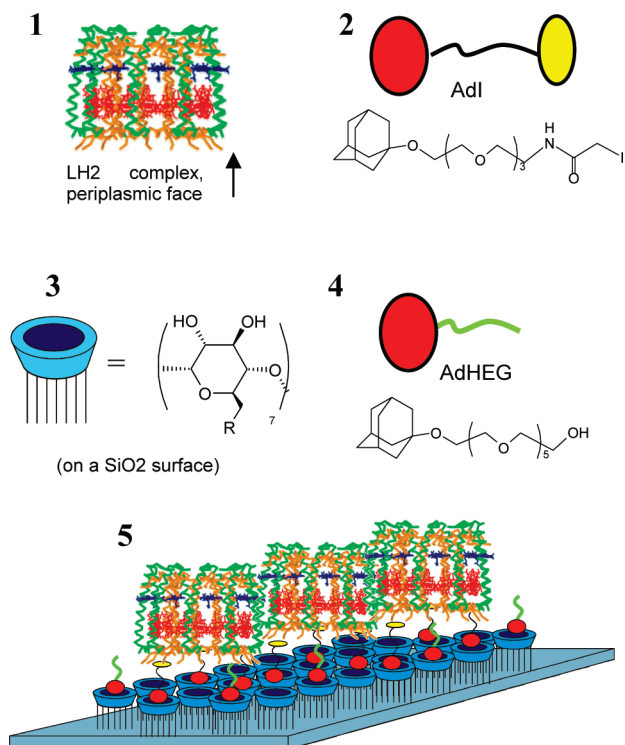
energy transport compared to the extent of transport in the absence of oxygen.

The LH2 complexes were solubilized from membranes from photosynthetically grown *Rb. sphaeroides* using 4% *N,N*-dimethyldodecylamine *N*-oxide (LDAO), purified on DEAE (Sigma) and Resource Q (GE Healthcare) columns, and then size fractionated on a Superdex 200 gel filtration column (GE Healthcare). The mutagenesis protocol has been described before.²³ LH2 complexes were crystallized as described in Walz et al.²⁴

For the fabrication of nanometer arrays of LH2 complexes, we used a recently reported approach based on a combination of site-directed mutagenesis, nanoimprint lithography (NIL) and multivalent host–guest interactions.²⁵ β -Cyclodextrin (β -CD), which acted as the host molecule, is a water-soluble cyclic oligosaccharide made of seven glucose units linked through α -1,4 bonds. This cone-shaped molecule exhibits a polar external face, while the interior of the cavity, containing two rings of C–H groups with a ring of glycosidic oxygen in between, is relatively nonpolar. LH2 complexes functionalized with the appropriate guest molecule can be positioned specifically on the β -CD modified substrate.

LH2 complexes were engineered with cysteine residues at the penultimate position of the C-terminus of the α -polypeptide chain, block 1, Chart 1. These strategic positions at the periplasmic face ensured a uniform orientation of the protein complexes upon binding to the surface. The cysteine residues were modified with iodoacetyl-tri(ethylene glycol) mono(adamantyl ether), AdI, block 2, Chart 1. LH2-protein in an aqueous buffered solution of 20 mM HEPES, pH 8.0, 0.03% *n*-dodecyl- β -D-maltoside (β -DDM) was mixed in 1:20 mol equiv with the AdI in 1.3% dimethyl sulfoxide (DSMO) to yield LH2 functionalized with adamantyl molecules, referred to as Ad_nLH2. When adsorbing Ad_nLH2 onto a β -CD-coated glass substrate (Chart 1, block 3), hexa(ethylene glycol) mono(adamantyl ether) AdHEG, block 4, served as a temporary blocking agent for the β -CD cavities, preventing

CHART 1. Representation of Host, Guest, and Target Molecules^a



^a Key: 1, a representation of an LH2 complex with the periplasmic face pointing down; 2, iodoacetyl-tri(ethylene glycol) mono(adamantyl ether);¹¹ 3, β-CD heptamine, host molecule; 4, hexa(ethylene glycol)-mono(adamantyl ether) (AdHEG); 5, Ad_nLH2 on the β-CD monolayer.

nonspecific adsorption by shielding the surface with the HEG chain. The monovalent AdHEG is later effectively displaced through competition by exploiting the higher affinity of the multivalent Ad_nLH2.²⁶

NIL was used to chemically pattern substrates with active β-CD monolayers to specifically bind Ad_nLH2. The complementary areas were passivated with poly(ethylene glycol).²⁷ NIL was performed using stamps with silicon ridges as small as 40 nm and a 4 μm period.²⁸ In this way the patterned LH2 structures approach molecular dimensions. Details of the fabrication process are described in the Supporting Information, Figure S1. The assembly on the patterned surface is depicted in block 5, Chart 1.

We used an atomic force and fluorescence microscope²⁹ to characterize the antenna arrays in liquid conditions. For AFM imaging standard silicon nitride cantilevers with a length of 85 μm, force constant of 0.5 N/m, and resonance frequency between 25 and 35 kHz in liquid (ThermoMicroscopes, Sunnyvale, CA) were used. AFM images were obtained using tapping mode. Images contained 512 × 512 pixels and were recorded at a line scanning frequency of 2–4 Hz. Topographical images were quantitatively analyzed using the scanning probe image processor (SPIP) software (Image Metrology ApS, Lyngby, Denmark). Fluorescence spectral microscopy was performed using 800 nm light from a diode laser (Roithner Laser Technik, RLT80010MG). The

excitation powers were sufficiently low to ensure that the chance of annihilation of singlet excitation could be neglected.³⁰ The laser beam is reflected from the dichroic beam splitter (Chroma, Q850LPXXR) toward an oil-immersion objective (Nikon, Plan Fluor 100×, NA = 1.3), which focuses the light onto the sample. The fluorescence light is collected by the same objective and passes through the dichroic beam splitter. Two mirrors direct the fluorescence light either toward a single photon counting avalanche photodiode (APD) (SPCM-AQR-14, Perkin-Elmer Optoelectronics) or toward a custom designed prism-based spectrograph with single molecule sensitivity equipped with a liquid-nitrogen-cooled CCD camera (Spec-10:100B, Princeton Instruments) or to an imaging branch to record the image of the photoemission on a CCD camera (Paxis 400, Princeton Instruments). The imaging optics were designed such that 50 nm in object space (*x* and *y* direction) corresponded with one pixel (20 × 20 μm) on the camera. A schematic drawing of the instrument is available in the Supporting Information, Figure S2.

The concept of the experiment for direct observation of energy propagation on the LH2 structures is depicted in Figure 1. The fluorescence emission area, represented in orange, is collected on the CCD camera and compared with the laser beam reflected from a passive surface, represented by the blue colored area. For a 2D structure such as the lipid reconstituted LH2 2D crystals (Figure 1a), energy could propagate radially away from the excitation area, as indicated by the green arrows in Figure 1a. In geometrically confined structures, such as line arrays of LH2 complexes, with a width much smaller than the area excited by the laser beam, as shown in Figure 1b, excitonic transport will be confined by the specific geometry of the array. The accuracy of far field fluorescence microscopy in determining the fluorescence emission area is only dependent on the signal-to-noise ratio and is therefore perfectly able to detect and determine the extent of excitation transfer.

Panels a and b of Figure 2 show AFM height images in liquid of Ad_nLH2 complexes on a β-CD SAM. The mean full width at half-maximum (fwhm) of the lines after processing (Supporting Information) is 80 ± 5 nm with a height of ~7 ± 1 nm (Figure 2e), consistent with the assembly of a monolayer of LH2 complexes. Figure 2c shows a fluorescence image of the engineered nanoarrays with a uniform intensity distribution along the lines (standard deviation of 4%). The sample was spectrally characterized in each pixel. Quantitatively, the spectral response from the immobilized Ad_nLH2 complexes, Figure 2f, showed no visible shift of the emission maximum at ~868 nm (filled black squares), with respect to bulk measurements of nonmodified LH2 complexes indicated by the gray filled area. We conclude that the structural integrity of the LH2 membrane proteins is preserved by this method of patterning. We also selected lipid reconstituted LH2 crystals for energy transport experiments. Figure 2d shows an AFM topography image of 2D

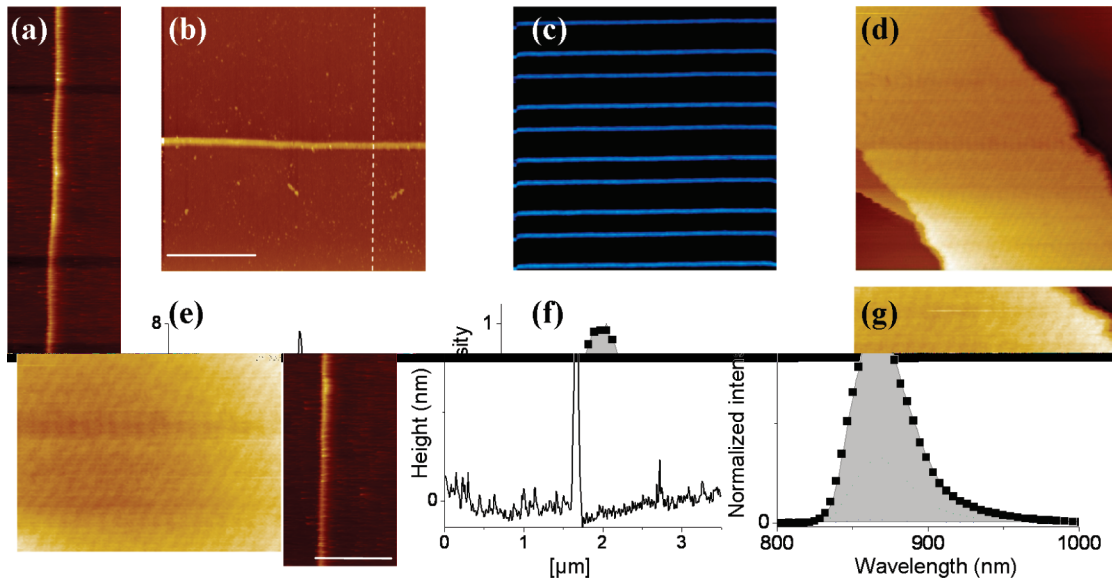


FIGURE 2. (a, b) AFM topography images and (e) cross section of patterned Ad_nLH2 on β-CD/PEG SAM (scale bar 1 μ m). (c) False color fluorescence image of the patterned Ad_nLH2 complexes, frame 39 \times 39 μ m. (f) Emission spectrum from patterned Ad_nLH2 (black squares) compared to LH2 in solution (gray area). (d) AFM topography LH2-only 2D crystal, frame 624 \times 624 nm. Packing in the crystal can be observed in panel (g), frame 120 \times 120 nm. The measurements were performed in liquid conditions.

LH2 crystals acquired under physiological conditions, while a higher resolution image of the crystal shows the periodic arrangement of the LH2 complexes (Figure 2g).

To detect energy migration in the LH2 assemblies, we proceeded to image the fluorescence emission after resonant excitation with laser light of 800 nm. LH2 crystal substrates were prepared by adsorbing 1 μ L of sample solution onto the surface of amino-functionalized glass cover slips for \sim 2 min, followed by rinsing with Milli-Q water in order to remove weakly bound crystal patches. The sample was immediately placed onto the characterization stage and kept liquid for imaging. Panels a, c, and e of Figure 3 show false color confocal fluorescence images of the different LH2 structures and the corresponding images (Figure 3b,d,f) of the fluorescence emission areas, after point excitation, as acquired with the imaging camera. A confocal fluorescence image of the 2D-LH2 crystals was acquired in order to locate their position on the glass support (Figure 3a). Subsequently, the laser beam was parked on a crystal and the fluorescence emission was imaged on the CCD camera (figure 3b). The fluorescence emission area was referenced against the area of the laser beam profile reflected from an inactive substrate, such as bare glass or a bleached LH2 crystal. In order to bleach a section of the LH2 crystal the laser beam was parked on a crystal until no LH2 fluorescence emission was detected in the spectrograph. A confocal fluorescence image of the bleached crystal is presented in Figure 3c (white arrow). The laser beam profile in reflection is displayed in Figure 3d. No difference was observed between the laser beam profile on a bleached LH2 crystal with respect to the profile on a glass-only area (fwhm 400 ± 50 nm). This observation indicates that the increase in dimension and shape of the fluorescence emission area after point illumina-

tion, which was measured on an intact LH2 crystal, demonstrates energy migration in the crystal. The comparison between previously bleached and unbleached crystals rules out contributions from scattering of the monolayers and LH2 molecules. Fluorescence imaging of the emission area was also performed on nanometer arrays of Ad_nLH2 complexes (Figure 3e,f). From Figure 3f, it can be observed that the fluorescence emission upon local excitation of the array becomes elongated and follows the architecture of the patterned protein nanoarray.

Figure 3g shows the intensity profiles of the fluorescence emission area measured along the y direction on the different substrates. The blue circles indicate the laser beam profile, the red squares the fluorescence profile on a lipid reconstituted 2D-LH2 crystal, and the green diamonds the profile of fluorescence emission from a nanometer array of LH2 complexes. These graphs were acquired at a laser intensity of 370 nW (measured at the back aperture of the objective). The measured diffraction limited spot size of the laser beam has a fwhm of 400 nm (Figure 2d). Since the dimension of the LH2 line array is approximately 80 nm in the y direction, Figure 2f, it is observed with the same diffraction limited width of 400 nm. For the case of the 2D-LH2-crystal, the fluorescence emission has a fwhm of \sim 900 nm \pm 50 nm. The profile of the fluorescence emission in the x direction for the 2D crystals and the laser beam is similar to that in the y direction as can be observed in Figure 3h. We conclude that energy migration results in a considerable broadening of the fluorescence emission area from the 2D-LH2 crystals.

A higher degree of energy transport is evident in the nanopatterned line array of LH2 complexes. The intensity profile in the x direction is depicted in Figure 3h. The fwhm

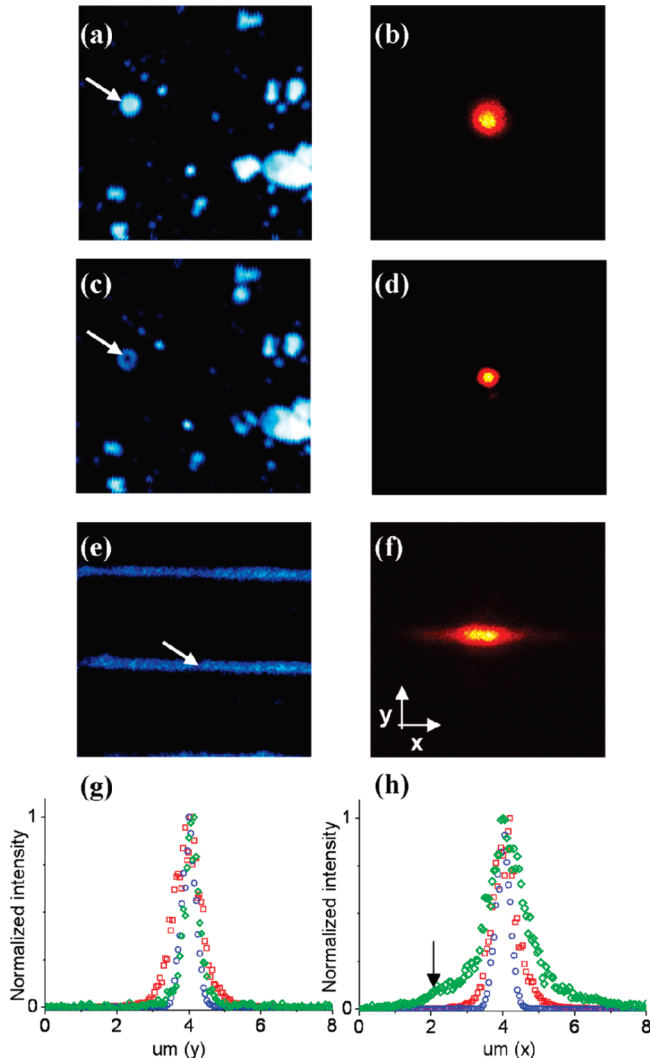


FIGURE 3. False color fluorescence confocal images of different LH2 substrates: (a) LH2-only 2D crystals, (c) LH2-only 2D crystals after photobleaching a section of the crystal indicated by the arrow, $40 \times 40 \mu\text{m}^2$, (e) bioengineered LH2-only nanoarray, $9 \times 9 \mu\text{m}^2$. Images of the fluorescence emission upon local excitation (b) LH2-only 2D crystals, (d) reference laser beam profile on photobleached LH2-only crystal, (f) bioengineered LH2-only nanoarray, $8 \times 8 \mu\text{m}^2$ (160×160 pixel). The respective fluorescence emission profile in *y* direction (g) and *x* direction (h); the arrow indicates a position $2 \mu\text{m}$ away from the center of the excitation point. LH2-only 2D crystals (red square); excitation laser (blue circle); LH2 nanometer arrays (green diamond shape). All measurements were performed in deoxygenated buffer.

of the fluorescence emission area of the nanometer arrays of LH2 upon local excitation increases to 1200 nm. Closer inspection of the emission profile reveals emission beyond 2000 nm, indicated by the arrow in Figure 3h, from the central excitation point.

If excitonic transport can be described as diffusional transport in the quasi-one-dimensional line array with a step size of ~ 6.8 nm, which is the diameter of an LH2 antenna protein, this would suggest that approximately $(2000 - 225/6.8)^2 \sim 6.8 \times 10^4$ steps are made before the excitation is spontaneously emitted from the assembly. ($\langle X^2(n) \rangle = d n \varepsilon^2$,

with d the dimension (1, 2, ...), n the number of steps, and ε the step size (6.8 nm for LH2.) Energy transfer between LH2 complexes has been predicted on the basis of a Förster transfer process to be of the order of picoseconds.³¹ Indeed, despite difficulties to determine LH2–LH2 transfer times, experimental evidence exists³² for the occurrence of fast, approximately 5 ps, dynamic events in assemblies of light harvesting systems. The fluorescence lifetime, τ_f , of the emission of single LH2 complexes is approximately 1–1.5 ns.^{30,33} A large number of steps, according to a diffusional transport process, suggests a transfer time of the excitation between individual pairs of LH2 molecules of the order of a few tens of femtoseconds in a considerable fraction of all transfer events. A recent three-photon echo experiment reported a transfer time of ~ 5 ps,³² which is within the range of existing theoretical estimates.³¹ Previous studies³⁰ on fluorescence decay kinetics of LH2 complexes in lipid reconstituted membranes reported a fast component of ~ 30 ps attributed to intercomplex energy transfer. It was proposed that the fast component was a result of efficient neighbor–neighbor interactions of the complexes in the phospholipid membrane.³⁰ Such a decrease in lifetime upon clustering of the LH2 complexes was not always accompanied by a significant shift in the fluorescence emission spectra. If we consider unidirectional transport, the time of excitation between different LH2 complexes ($(2000 - 225)/6.8 - 260$ complexes) is estimated to be near 5 ps, which is in agreement with reported values. These different observations might indicate not only that diffusional transport plays a role but also that unidirectional transport events occur.

Moment analysis of the intensity distribution along the LH2 assemblies was performed to facilitate a quantitative comparison of the extent of the energy migration in relation to the intensity distribution of the laser excitation beam. First, second, and third central moments were calculated according to eq 1 to compare the extent of transport in different experiments.

$$\mu_n(a) = \sum_i (x_i - a)^n P(x_i) \quad (1)$$

where $\mu_n(a)$ is the n th order moment around the maximum intensity centered in pixel a , x_i is the displacements in pixels from a , and $P(x_i)$ is the respective intensity value in the pixel x_i . We used the normalized ratio $\mu_n(a)_{\text{LH2assemblies}} / \mu_n(a)_{\text{Laser}}$ as a measure of energy transport in different sample geometries. The higher order moments in the moment analysis of the intensity profile are most prominent when the extent of the energy transport increases. The central moments ratios are presented in Table 1.

In the *x* direction, for the 2D-LH2 crystals, $\mu_2 > \mu_1$, and are 2.30 and 1.80, respectively. The deviation from unity indicates a broadening of the fluorescence emission area upon illumination of the 2D crystals. Although the third

TABLE 1. Ratio $\mu_n(a)_{\text{LH2assemblies}}/\mu_n(a)_{\text{Laser}}$ in x and y Directions (x , y)^a

	$\mu_n(a)_{\text{LH2assemblies}}/\mu_n(a)_{\text{Laser}}$		
	$\mu_1(x,y)$	$\mu_2(x,y)$	$\mu_3(x,y)$
LH2-only 2D crystal	1.8, 1.7	2.3, 2.0	1.3, 1.2
LH2 nanometer array	3.4, 1.0	6.1, 1.0	5.8, 1.0

^a $n = 1, 2, 3$.

moment μ_3 has a lower value than the second and first moment, the clear difference from unity indicates significant long-range energy transport. A more dramatic effect is observed for the nanometer line arrays. The magnitudes of the first three moments are much larger for nanometer line arrays of LH2 than for 2D-LH2 crystals, as displayed in Table 1. The LH2 crystals are, unlike the organization of LH2 complexes in natural membranes, composed of regular arrays of up- and down-oriented LH2 complexes.³⁴ The “up–down” arrangement reduces the efficiency of transfer as the distances between porphyrin B850 rings are increased. Since the transport distance per step is determined by the size of a LH2 unit, the competition between the rate of spontaneous emission and the decreased transfer rate will bias for smaller transfer distances in “up–down” vs “all up” (or “all down”) geometries, as in the quasi-linear arrays. The observed energy propagation in the quasi-1D nanometer LH2 complex arrays also suggests that the host–guest patterning approach leads to tight packing of protein complexes, since this is a requirement for efficient energy propagation.

It is well-known that the presence of oxygen affects the integrity of BChl molecules^{35,36} either through triplet state formation and subsequent oxidation by singlet oxygen or through direct oxidation of excited state BChl.^{37,38} The extent of energy transport was investigated in the presence of ambient concentrations of oxygen with the expectation that this would significantly reduce the observed exciton transport in arrays of light harvesting complexes. The oxygen level was reduced by nitrogen flushing to a level not detectable with an electrolytic oxygen meter (0.01 mg/L, Cyberscan 110, Eutech Instruments, Nijkerk, The Netherlands).

Parts a and b of Figure 4 show results of the degree of broadening on nanometer line arrays of LH2. The measurements were performed in ambient concentration of dissolved oxygen in the buffer and in deoxygenated buffer, respectively. The fwhm of the fluorescence emission area measured along the nanometer arrays of LH2 complexes is $1.1 \pm 0.1 \mu\text{m}$ when measured in deoxygenated buffer (Figure 4a, red circles) as compared to $0.4 \mu\text{m}$ for a reflected beam (blue circles). In ambient dissolved oxygen conditions, the corresponding fwhm of the fluorescence emission area is $0.7 \pm 0.1 \mu\text{m}$ (Figure 4b, black circles). This result confirms our expectation that the presence of oxygen reduces the extent of energy transport. A cumulative intensity plot of the intensity profile of the fluorescence emission, Figure 4c,

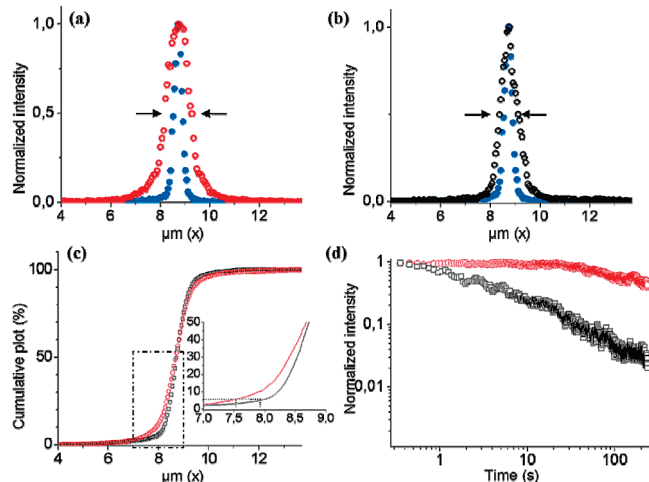


FIGURE 4. Intensity profile of the fluorescence emission area on nanometer arrays of $\text{Ad}_n\text{LH2}$ compared with the excited area (solid dark blue circles), excitation power 80 nW: (a) oxygen reduced, open red circles; (b) ambient oxygen concentration, open black circles, the arrows indicate the fwhm; (c) cumulative intensity plot of transport in the absence (red open circles) and the presence (black open circles) of oxygen. The inset is a magnification of the rectangular box. (d) Fluorescence time trace on the nanometer arrays of $\text{Ad}_n\text{LH2}$, in the absence (red) and the presence (black) of oxygen.

indicates that approximately 10 % of the energy propagation events occur at a distance up to 1260 nm from the center of the excitation beam in the absence of oxygen. In the presence of oxygen this distance shortens to 700 nm. The effect of oxygen is further demonstrated in Figure 4d, which shows fluorescence time traces on nanometer line arrays in the absence (red) and presence (black) of oxygen at low excitation power. From the curve it can be observed that photobleaching in the absence of oxygen is absent up to about 20 s. It can be concluded that bleaching does not affect the fluorescence images (Figure 3), which are acquired in 100 ms.

By selectively creating optical interruptions for the excitonic transport on the patterned nanoarrays, we could observe directionality in the propagation direction. The laser line was parked on an array of LH2 and defects (dimensions of few hundred nanometers corresponding to the size of the confocal spot) were created by photobleaching due to prolonged exposure to the laser beam in order to hamper the energy migration process through those areas. We then proceeded to excite the nanometer array by positioning the beam slightly to the left and to the right of the induced defect with the scan stage. The images of the fluorescence emission areas on the arrays are shown in parts a and b of Figure 5, respectively. Figure 5c shows the intensity profile along the patterned arrays. From the profiles a directional propagation of energy can be directly observed, as light does not propagate through the defect area. Transport in either direction can be observed just depending on which side of the defect area the molecular antenna array is excited. The red circles show the case of illumination on the left and propagation to the left and the opposite direction is observed when the laser

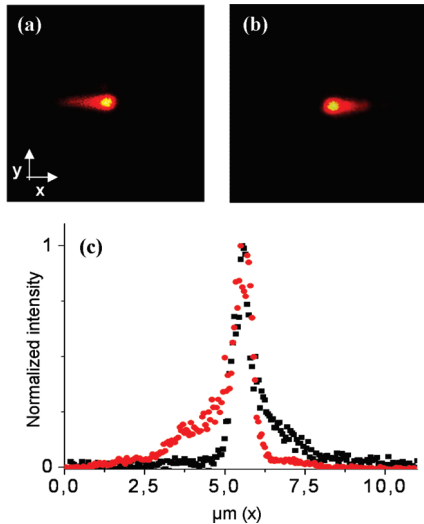


FIGURE 5. The effect of a defect on energy propagation. Images of the fluorescence emission areas when the excitation laser beam is positioned at the (a) left side or (b) right side of the defect. The defect was intentionally created through photobleaching of an area on the line array with the laser beam. Energy migration can be observed to follow the direction of the line. (c) Intensity distribution from panel (a) filled red circles, left, and (b) filled black squares, right.

beam is placed toward the right of the defect, as is illustrated by the filled black square curve in Figure 5c.

In summary, we report, for the first time, a direct observation of long-range energy migration in bioengineered, closely packed arrays of LH2 antenna complexes. The spatial extent of transport was determined by an analysis of the fluorescence emission areas and comparison with the excitation area of the laser beam. Experimental data showed evidence of excitonic transport in 2D-LH2 crystals and on nanometer line arrays of LH2 complexes. In comparison with the natural arrangement of the antenna complexes in photosynthetic organisms,³⁹ which does not require long-distance transport, we have observed unprecedented energy propagation distances on the bioengineered nanometer arrays. These results demonstrate the potential of using natural antennas from photosynthetic organisms in hybrid systems for long-range energy propagation. In a wider context, these results may have a profound impact on strategies to harvest and transport solar energy in devices for sustainable energy production. These concepts will be further explored in future experiments, which include more complex architectures and time-resolved optical measurements.

Acknowledgment. We thank the Nanotechnology Network in The Netherlands (NanoNed), for financial support, project number TMM.7124. Y.Z. acknowledges funding from MESA+ (SRO-NF). C.N.H. acknowledges funding from the BBSRC, U.K.

Supporting Information Available. Materials, schematic of the setup, details of nanoimprint lithography process, and chemical functionalization. This information is available free of charge via the Internet at <http://pubs.acs.org>

REFERENCES AND NOTES

- (1) Govorov, A. O.; Carmeli, I. *Nano Lett.* **2007**, *7* (3), 620–625.
- (2) Das, R.; Kiley, P. J.; Segal, M.; Norville, J.; Yu, A. A.; Wang, L.; Trammell, S. A.; Reddick, L. E.; Kumar, R.; Stellacci, F.; Lebedev, N.; Schnur, J.; Bruce, B. D.; Zhang, S.; Baldo, M. *Nano Lett.* **2004**, *4* (6), 1079–1083.
- (3) Escalante, M.; Maury, P.; Bruinink, C. M.; van der Werf, K.; Olsen, J. D.; Timney, J. A.; Huskens, J.; Hunter, C. N.; Subramaniam, V.; Otto, C. *Nanotechnology* **2008**, *19*, (2), -.
- (4) Reynolds, N. P.; Janusz, S.; Escalante-Marun, M.; Timney, J.; Ducker, R. E.; Olsen, J. D.; Otto, C.; Subramaniam, V.; Leggett, G. J.; Hunter, C. N. *J. Am. Chem. Soc.* **2007**, *129* (47), 14625–14631.
- (5) Trammell, S. A.; Wang, L.; Zullo, J. M.; Shashidhar, R.; Lebedev, N. *Biosens. Bioelectron.* **2004**, *19* (12), 1649–1655.
- (6) Nakamura, C.; Hasegawa, M.; Nakamura, N.; Miyake, J. *Biosens. Bioelectron.* **2003**, *18* (5–6), 599–603.
- (7) Hunter, C. N.; Daldal, F.; Thurnauer, M. C.; Beatty, J. T. *The Purple Phototropic Bacteria*; Springer: Dordrecht, 2008; Vol. 28.
- (8) Vangrondelle, R.; Dekker, J. P.; Gillbro, T.; Sundstrom, V. *Biochim. Biophys. Acta* **1994**, *1187* (1), 1–65.
- (9) McDermott, G.; Prince, S. M.; Freer, A. A.; Hawthornthwaitelawless, A. M.; Papiz, M. Z.; Cogdell, R. J.; Isaacs, N. W. *Nature* **1995**, *374* (6522), 517–521.
- (10) Scheuring, S.; Seguin, J.; Marco, S.; Leivy, D.; Breyton, C.; Robert, B.; Rigaud, J. L. *J. Mol. Biol.* **2003**, *325* (3), 569–580.
- (11) Fotiadis, D.; Qian, P.; Philipsen, A.; Bullough, P. A.; Engel, A.; Hunter, C. N. *J. Biol. Chem.* **2004**, *279* (3), 2063–2068.
- (12) Qian, P.; Hunter, C. N.; Bullough, P. A. *J. Mol. Biol.* **2005**, *349* (5), 948–960.
- (13) Sundström, V.; Pullerits, T.; Van Grondelle, R. *J. Phys. Chem. B* **1999**, *103* (13), 2327–2346.
- (14) Van Grondelle, R.; Novoderezhkin, V. I. *Phys. Chem. Chem. Phys.* **2006**, *8* (7), 793–807.
- (15) Pullerits, T.; Sundstrom, V. *Acc. Chem. Res.* **1996**, *29* (8), 381–389.
- (16) Cogdell, R. J.; Gardiner, A. T.; Roszak, A. W.; Law, C. J.; Southall, J.; Isaacs, N. W. *Photosynth. Res.* **2004**, *81* (3), 207–214.
- (17) Herek, J. L.; Wohlleben, W.; Cogdell, R. J.; Zeidler, D.; Motzkus, M. *Nature* **2002**, *417* (6888), 533–535.
- (18) Cogdell, R. J.; Gall, A.; Kohler, J. Q. *Rev. Biophys.* **2006**, *39* (3), 227–324.
- (19) Sener, M. K.; Olsen, J. D.; Hunter, C. N.; Schulten, K. *Proc. Natl. Acad. Sci. U.S.A.* **2007**, *104* (40), 15723–15728.
- (20) Scheuring, S.; Sturgis, J. N.; Prima, V.; Bernadac, A.; Levy, D.; Rigaud, J. L. *Proc. Natl. Acad. Sci. U.S.A.* **2004**, *101* (31), 11293–11297.
- (21) Bahatyrova, S.; Frese, R. N.; Siebert, C. A.; Olsen, J. D.; van der Werf, K. O.; van Grondelle, R.; Niederman, R. A.; Bullough, P. A.; Otto, C.; Hunter, C. N. *Nature* **2004**, *430* (7003), 1058–1062.
- (22) Scheuring, S.; Sturgis, J. N. *Science* **2005**, *309* (5733), 484–487.
- (23) Olsen, J. D.; Robert, B.; Siebert, C. A.; Bullough, P. A.; Hunter, C. N. *Biochemistry* **2003**, *42* (51), 15114–15123.
- (24) Walz, T.; Jamieson, S. J.; Bowers, C. M.; Bullough, P. A.; Hunter, C. N. *J. Mol. Biol.* **1998**, *282* (4), 833–845.
- (25) Escalante, M.; Zhao, Y. P.; Ludden, M. J. W.; Vermeij, R.; Olsen, J. D.; Berenschot, E.; Hunter, C. N.; Huskens, J.; Subramaniam, V.; Otto, C. *J. Am. Chem. Soc.* **2008**, *130* (28), 8892.
- (26) Ludden, M. J. W.; Mulder, A.; Tampe, R.; Reinoudt, D. N.; Huskens, J. *Angew. Chem., Int. Ed.* **2007**, *46* (22), 4104–4107.
- (27) Kannan, B.; Castelino, K.; Chen, F. F.; Majumdar, A. *Biosens. Bioelectron.* **2006**, *21* (10), 1960–1967.
- (28) Zhao, Y.; Berenschot, E.; Jansen, H.; Tas, N.; Huskens, J.; Elwenspoek, M. *Microelectron. Eng.* **2009**, *86* (4–6), 832–835.
- (29) Kassies, R.; Van der Werf, K. O.; Lenferink, A.; Hunter, C. N.; Olsen, J. D.; Subramaniam, V.; Otto, C. *J. Microsc. (Oxford, U.K.)* **2005**, *217*, 109–116.
- (30) Pflock, T.; Dezi, M.; Venturoli, G.; Cogdell, R. J.; Kohler, J.; Oellerich, S. *Photosynth. Res.* **2008**, *95* (2–3), 291–298.
- (31) Ritz, T.; Damjanovic, A.; Schulter, K. *ChemPhysChem* **2002**, *3* (3), 243–248.
- (32) Agarwal, R.; Rizvi, A. H.; Prall, B. S.; Olsen, J. D.; Hunter, C. N.; Fleming, G. R. *J. Phys. Chem. A* **2002**, *106* (33), 7573–7578.

- (33) Chen, X. H.; Zhang rname>, L.; Weng, Y. X.; Du, L. C.; Ye, M. P.; Yang, G. Z.; Fujii, R.; Rondonuwu, F. S.; Koyama, Y.; Wu, Y. S.; Zhang, J. *P Biophys. J.* **2005**, *88* (6), 4262–4273.
- (34) Bahatyrova, S.; Frese, R. N.; van der Werf, K. O.; Otto, C.; Hunter, C. N.; Olsen, J. D. *J. Biol. Chem.* **2004**, *279* (20), 21327–21335.
- (35) Rutkauskas, D.; Novoderezhkin, V.; Cogdell, R. J.; van Grondelle, R. *Biochemistry* **2004**, *43* (15), 4431–4438.
- (36) Rutkauskas, D.; Novoderezhkin, V.; Cogdell, R. J.; van Grondelle, R. *Biophys. J.* **2005**, *88* (1), 422–435.
- (37) Law, C. J.; Cogdell, R. J. *FEBS Lett.* **1998**, *432* (1–2), 27–30.
- (38) Bopp, M. A.; Sytnik, A.; Howard, T. D.; Cogdell, R. J.; Hochstrasser, R. M. *Proc. Natl. Acad. Sci. U.S.A.* **1999**, *96* (20), 11271–11276.
- (39) Olsen, J. D.; Tucker, J. D.; Timney, J. A.; Qian, P.; Vassilev, C.; Hunter, C. N. *J. Biol. Chem.* **2008**, *283* (45), 30772–30779.